Patient-Specific Computational Modeling of Different Cannulation Strategies for Extracorporeal Membrane Oxygenation

Yunus Ahmed,*† Sabrina R. Lynch,‡ Jonathan W. Haft,* Frans L. Moll,† Joost A. van Herwaarden,† Nicholas S. Burris,§ Himanshu J. Patel,* and C. Alberto Figueroa‡¶

Abstract: Institution of extracorporeal membrane oxygenation (ECMO) results in unique blood flow characteristics to the end-organ vascular beds. We studied the interplay between cardiac-driven and extracorporeal membrane oxygenation (ECMO)-driven flow to vascular beds in different ECMO configurations using a patient-specific computational fluid dynamics (CFD) analysis. A computational ECMO model (femoral artery cannulation [FAC]) was constructed using patient-specific imaging and hemodynamic data. Following model calibration, we augmented the 3D geometrical model to represent alternative ECMO configurations (ascending aorta cannulation [AAC] and subclavian artery cannulation [SAC]). We performed CFD analyses, including a novel virtual color-dye analysis to compare global and regional blood flow and pressure characteristics as well as contributions of cardiac and ECMO-derived flow to the various vascular beds. Flow waveforms at all the aortic branch vessels were pulsatile, despite low cardiac output and predominant nonpulsatile ECMO-driven hemodynamics. Virtual color-dye analysis revealed differential contribution of cardiac and ECMO-derived flow to the end-organ vascular beds in the FAC model, while this was more evenly distributed in the AAC and SAC models. While global hemodynamics were relatively similar between various ECMO configurations, several distinct hemodynamic indices, in particular wall shear stress and oscillatory shear patterns, as well as differential contribution of ECMO-derived flow to various vascular beds, showed remarkable differences. The clinical impact of this study highlighting the relevance of CFD modeling in assessment of complex hemodynamics in ECMO warrants further evaluation. *ASAIO Journal* 2022; 68;e179–e187

Key Words: extracorporeal membrane oxygenation, computational fluid dynamics, patient-specific modeling, virtual color-dye analysis

Extracorporeal membrane oxygenation (ECMO) has proven to be an effective treatment modality in patients presenting with acute cardiopulmonary distress. Since its introduction in 1977, use of ECMO has increased, and may even show great potential in the treatment of COVID-19 related complications.[1,2] Several cannulation strategies for ECMO exist.[3] Veno-venous (VV)-ECMO is used to treat isolated pulmonary failure by bypassing the lungs. Venoarterial (VA)-ECMO, providing complete cardiopulmonary support, is widely used in patients presenting with postcardiotomy syndrome, cardiogenic shock following myocardial infarction, or as a bridge to recovery, transplantation, or ventricular assist device (VAD) placement. Adult VA-ECMO can be instituted in a central fashion in which the arterial cannula is placed directly into the ascending aorta, or through a peripheral fashion where the arterial cannula is placed in the femoral, axillary or subclavian arteries. Complications of VA-ECMO vary with the cannulation strategy and include kidney failure, pulmonary congestion, bleeding, limb ischemia, infection, or stroke.[4]

Choice of ECMO cannulation strategies in adults is dependent various factors, including size of the access vessels, patient risk profile, need for cardiopulmonary resuscitation, setting of postcardiotomy shock (PCS), need for rapid deployment,

From the *Department of Cardiac Surgery, University of Michigan, Ann Arbor, Michigan; †Department of Vascular Surgery, University Medical Center Utrecht, Utrecht, Netherlands; ‡Department of Biomedical Engineering, University of Michigan, Ann Arbor, Michigan; §Department of Radiology, University of Michigan, Ann Arbor, Michigan; ¶Department of Surgery, University of Michigan, Ann Arbor, Michigan.

Submitted for consideration October 2021; accepted for publication in revised form August 2022.

Disclosures: The authors have no conflicts of interest to report.

This work was support by an Extreme Science and Engineering Discovery Environment (XSEDE) grant, National Science Foundation grant number ACI-1548562. N.S.B. received from Radiologic Society of North America Research Scholar Grant (RSCH 1801) & National Institutes of Health (R44 HL145953). H.J.P. received from Joe D. Morris Professorship; David Hamilton Fund and the Phil Jenkins Breakthrough Fund. C.A.F. received from Edward B. Diethrich Professorship; the Bob and Ann Aikens Aortic Grants Program and the Frankel Cardiovascular Center.

Supplemental digital content is available for this article. Direct URL citations appear in the printed text, and links to the digital files are provided in the HTML and PDF versions of this article on the journal's Web site (www.asaiojournal.com).

Y.A. did conceptualization; data curation; formal analysis; investigation; methodology; project administration; resources; software; validation; visualization; writing—original draft; writing—review and editing. S.R.L. did conceptualization; formal analysis; investigation; methodology; project administration; resources; software; validation; visualization; writing—original draft; writing—review and editing. J.W.H. did conceptualization; data curation; supervision; writing—review and editing. F.L.M. did conceptualization; supervision; writing—review and editing. J.A.v.H. did conceptualization; supervision; writing—review and editing. N.S.B. did conceptualization; supervision; writing—review and editing. H.J.P. did conceptualization; data curation; methodology; project administration; resources; supervision; writing—review and editing. C.A.F. did conceptualization; data curation; formal analysis; funding acquisition; investigation; methodology; project administration; resources; software; supervision; validation; visualization; writing—original draft; writing—review and editing.

The data underlying this article will be shared on reasonable request to the corresponding author.

Correspondence: Yunus Ahmed, Department of Cardiac Surgery, University of Michigan Frankel Cardiovascular Center, 1500 E Medical Center Drive, 48109 Ann Arbor, MI. E-mail: yunahmed@gmail.com; Twitter: @yunahmedumich.

DOI: 10.1097/MAT.0000000000001819

and potential for long ECMO support.[5,6] While the guidelines stipulate advantages and disadvantages regarding various modes of ECMO management, the optimal cannulation strategy still remains unclear. Previous studies have not been able to demonstrate a clear survival benefit related to a particular mode of arterial cannulation, although a recent analysis of the Extracorporeal Life Support Organization Registry suggested a survival benefit for peripheral cannulation in patient presenting with PCS.[7–9] Additionally, there remains a gap in knowledge regarding the hemodynamic implications of these various cannulation strategies.[10] The pulsatile flow conditions imposed by the contractility of the heart are intrinsically different from the nonpulsatile ECMO flow.[11] Steady-state flow is known to alter microcirculatory processes and can lead to end- organ damage, most notably in the renal and cerebral microvasculature.[12,13] Although hemodynamic support with ECMO is able to restore global perfusion, abnormal flow conditions persist. This interplay between pulsatile cardiac and steady-state ECMO flow results in regions involving high shear flows, abnormal pulsatility, and differential perfusion pressures.[14] A thorough understanding of both global and regional blood pressure and flow phenomena in different cannulation configurations will aid in patient-specific decision making in ECMO management.

Computational fluid dynamics (CFD) is an established modeling technique that has been extensively used to study hemodynamics of cardiovascular diseases.[15] As such, CFD can be used to provide in-depth hemodynamic assessments in patients undergoing ECMO. This computational analysis technique combines patient-specific clinical data relating to anatomy, pressure and flow with advanced modeling tools to provide a noninvasive assessment of global and regional hemodynamic indices. Recent applications of CFD have proven a useful clinical tool within the cardiovascular field, aiding in surgical planning, and assessing the patient-specific hemodynamics effects of planned interventions.[16,17] More specifically, CFD analyses have been used to provide a mechanistic interpretation of ECMO, including the impact of varying flow rates on differential hypoxemia, flow mixing phenomena, and neurological complications related to ECMO.[18–22] In this work on adult ECMO, we evaluated global and regional hemodynamics in a 56-year-old patient on peripheral VA-ECMO following acute cardiopulmonary failure using a patient-specific CFD analysis, where we explored the hemodynamic alterations introduced by different ECMO configurations, and identified contributions of pulsatile cardiac and nonpulsatile ECMO flows to various end-organ vascular beds.

Materials and Methods

Ethical Statement

This computational analysis was performed as part of an Institutional Review Board of the University of Michigan approved study (ID #HUM00155491), on January 15, 2019, and written patient informed consent was waived.

Patient's History

A 56-year-old female, with a past medical history that included nonischemic cardiomyopathy and a nephrectomy, presented to our institution with unstable ventricular tachycardia. Following evaluation, the patient required hemodynamic support and an implantable cardiac defibrillator, and ECMO therapy was initiated. A 15 Fr arterial cannula was placed in the left femoral artery, and a 25 Fr venous cannula was placed in the right femoral vein and threaded into the IVC. To ensure distal limb perfusion, a 7 Fr femoral arterial cannula was placed distal to the primary arterial cannulation site. Following 10 days of ECMO hemodynamic support, a Heartware VAD system was implanted, and the patient was placed on the cardiac transplant list.

Clinical Data Acquisition

Anatomical data was obtained from an ECG-gated computed tomography (CT) angiography scan (slice thickness 1.25 mm, 120 mL intravenous contrast material). Native cardiac flow (1.08 L/min) information was acquired through duplex echocardiography of the left ventricle (LV). ECMO flow rate (3.4 L/min) at the time of the imaging study, including the distal perfusion catheter flow rate (0.25 L/min), was retrieved from the electronic patient chart. An invasive pressure catheterization performed at the right femoral artery provided information on aortic pressure (98/63 mmHg).

Computational Analysis

Patient-specific CFD simulations were performed to study hemodynamic alterations related to different ECMO configurations. Using available clinical imaging data for the patient, a 3D aortic model was constructed with the cardiovascular blood flow simulation software CRIMSON.[23] The 3D geometrical model, including the arterial ECMO cannula (thickness of 1 mm) and distal perfusion catheter inserted into the left femoral artery, was then discretized into a finite-element mesh consisting of 7,386,497 tetrahedral elements. The steps to creating the 3D mesh are shown in **Figure 1**. Then, this 3D geometry was augmented to represent the ascending aorta (3,941,182 tetrahedral elements) and subclavian artery (2,805,606 tetrahedral elements) cannulation configurations (**Figure 2**).

A 3D-0D open-loop computational model was used to reproduce regional blood flows and pressures within the ECMO circulations (**Figure 3**). A pulsatile, patient-specific waveform (1.08 L/min) derived from duplex echocardiography, was imposed at the ascending aortic inflow. The ECMO flow was imposed using a steady-state waveform (3.4 L/min) at inlet of the arterial ECMO cannula. To model the continuous flow through the distal perfusion catheter, a steady-state waveform (0.25 L/min) was imposed at the catheter outlet. Three-element Windkessel models, consisting of resistors and capacitors, were coupled to the various branch vessels to represent the distal vasculature. Using 1D theory formulations as published by Xiao et al, we set up the initial values for lumped parameter models (LPM) using a fix-point iteration strategy. We then tuned the LPM values for each branch in a series of 3D CFD analyses to match our flow splits and patient-specific data on pressure derived from right femoral artery catheterization. The model was deemed calibrated if flow and pressure (systolic, diastolic and pulse pressure) values were within 5% of our clinical and literature data.[24,25] The calibrated LPM values are reported in **Table 1**.

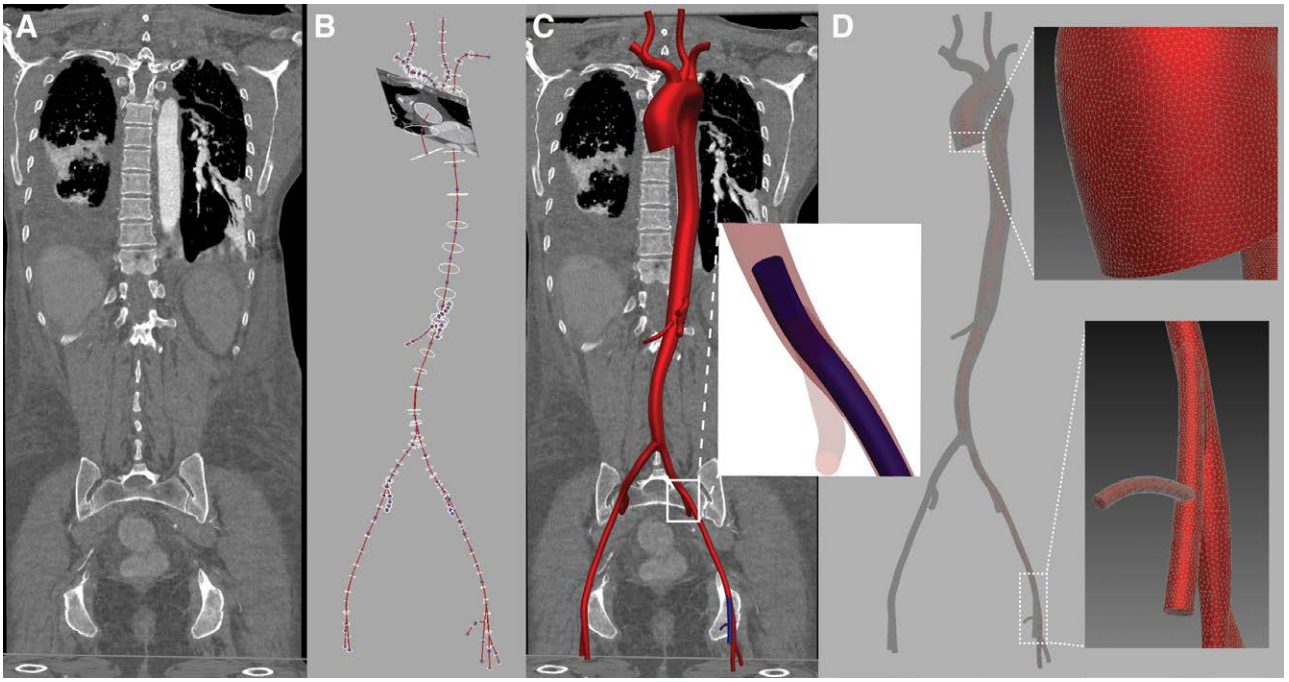

Figure 1. A patient-specific geometrical model of the aorta was constructed CTA data using the CRIMSON software. (A) CTA data of chest, abdomen, and pelvis. (B) 3D path lines were created and 2D contours were made to delineate the vessel walls. (D) Lofting and blending processes were used to create the 3D anatomical model, including an arterial ECMO canula inserted into the left femoral artery. (D) The anatomical model was discretized to create a finite-element mesh consisting of tetrahedral elements. CTA, computed tomography angiography; ECMO, extracorporeal membrane oxygenation.

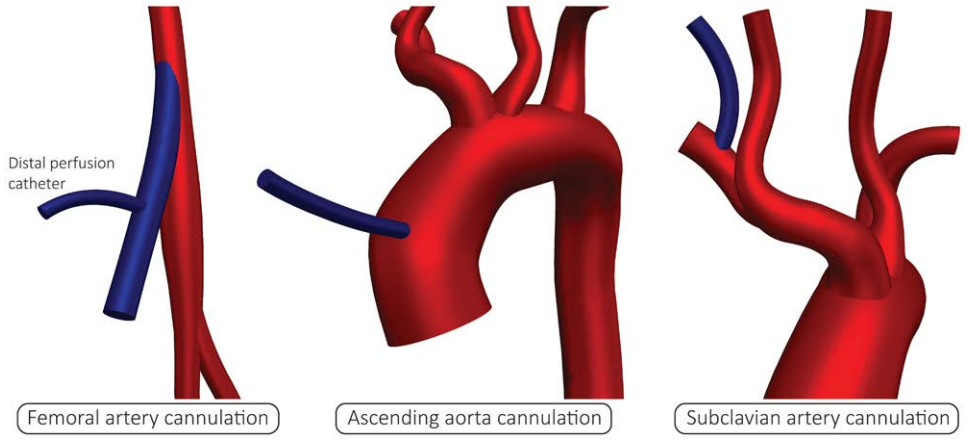

Figure 2. We created three different ECMO cannulation configurations. The arterial cannula is depicted in blue. ECMO, extracorporeal membrane oxygenation.

Following successful parameter calibration of the femoral artery cannulation (FAC) model, we ran blood flow simulations for the ascending aorta cannulation (AAC) and the subclavian artery cannulation (SAC) models. The boundary conditions for all the computational models were kept constant to study hemodynamic alterations introduced by the different ECMO cannulation strategies. Hemodynamic indices of interest included flow distribution, pressure, and wall shear stress (WSS). The time-averaged magnitude of the WSS (TAWSS) was defined as

$$\mathrm{TAWSS} = \left| \frac{1}{T} \int_0^T \tau_w dt \right|,$$

where T is the duration of one cardiac cycle and τ_w is WSS.[26] To asses complex flow patterns within our ECMO vascular domains, we additionally calculated the oscillatory shear index (OSI). This parameter has been able identify pro-atherogenic regions, and is defined as

$$\mathrm{OSI} = \frac{1}{2}\left(1 - \frac{\left|\int_0^T \tau_w \mathrm{d}t\right|}{\int_0^T |\tau_w|\,\mathrm{d}t}\right).$$

OSI can range from 0, depicting a region of unidirectional flow, to a maximum of 0.5, depicting a region of forward and back flow patterns.[27]

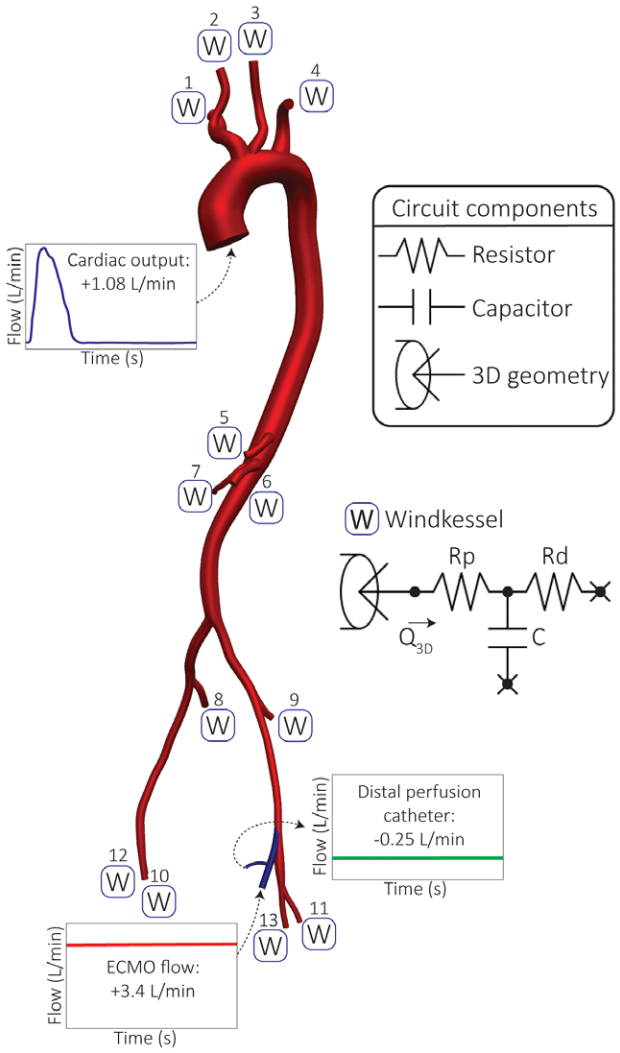

Figure 3. A 3D-0D open-loop model was constructed. A pulsatile aortic inflow waveform was imposed at the ascending aorta. A steady-state flow waveform was imposed at the ECMO arterial cannula. Flow through the distal perfusion catheter was modeled by imposing a steady-state waveform at the outlet. Three-element Windkessel models, consisting of resistances and capacitors, were coupled to all outflow branches to represent the distal vasculature. Numbering of the Windkessel models corresponds to the parameters listed in Table 1. C, capacitor; ECMO, extracorporeal membrane oxygenation; Rp, proximal resistor, Rd, distal resistor.

Virtual Color-dye Analysis

To visualize and quantify the contributions of pulsatile, cardiac-driven flow, and nonpulsatile ECMO-driven flow to the end-organ vascular beds, we employed a novel virtual color-dye analysis.[28] In this computational technique, the advection and diffusion equations were solved to obtain the spatiotemporal distribution of the concentration of two virtual dyes until cycle-to-cycle periodicity was achieved. The cardiac flow originating from the LV and the ECMO flow originating from the inlet of the arterial cannula were each tagged with an individual virtual dye with a concentration of 10 mols/mm^3. As blood flows through the circulation, the virtual dyes were transported throughout the models and were captured and quantified at the outlets. We were then able to quantify the contributions of pulsatile flow from the LV versus nonpulsatile flow from the ECMO cannula to all aortic branch vessels. For visualization purposes, the cardiac dye is labeled blue and the ECMO dye is labeled red.

Simulations were conducted using CRIMSON's Navier-Stokes flow solver on approximately 100 crores on the XSEDE platform and the University of Michigan's high-performance computing (HPC) cluster Conflux. Blood was modeled as an incompressible Newtonian fluid with a density of 1.06 g/cm^3 and a viscosity of 0.004 Pa·s. The aortic wall was modeled as rigid. Computational time per cardiac cycle was 36–48 hours, depending on the number of mesh elements in a geometrical model. Simulations were run until cycle-to-cycle periodicity in hemodynamic results was achieved. For the virtual color-dye analysis, simulations were run for 20–30 cycles before fully developed solutions were achieved.

Results

Patient-specific Model Calibration

We successfully reproduced patient-specific hemodynamics in the FAC model (**Figure 4**). Following iterative Windkessel parameter calibrations, our simulation results matched available literature data on cerebral, visceral and extremity blood flow within 5%. Systolic, diastolic and pulse pressure was matched exactly to clinical patient-specific invasive pressure catheterization data acquired at the right femoral artery.

Assessment of Hemodynamics in Different ECMO Configurations

In the patient-specific FAC model, we observed complex flow patterns throughout the thoracoabdominal aorta, as depicted in **Figure 5**, left panel. The peak-systolic velocity profile at the level of the descending thoracic aorta was entirely antegrade, while the mid-diastolic velocity profile was completely retrograde. At the distal abdominal aorta, the peak-systolic velocity profile revealed both antegrade and retrograde velocity magnitudes. The velocity profile at mid-diastolic velocity profile was complex, although entirely retrograde. Disturbed flow was identified near the iliac bifurcation, due to the high-velocity, steady-state flow from the ECMO cannula. The flow waveforms at the level of the descending thoracic aorta and supraceliac aorta were identical and revealed pulsatile, antegrade flow throughout systole, while flow was retrograde in diastole (**Figure 5**, right panel, green lines). Conversely, the flow waveform at the level of the infrarenal aorta was retrograde throughout the entire cardiac cycle with diminished pulsatility.

In the AAC model, disturbed flow was observed at the ascending aorta and aortic arch (**Figure 5**, left panel). Peak-systolic velocity profiles through the thoracoabdominal aorta were antegrade, as were the velocity profiles at mid-diastole, although of lower magnitude. The flow waveforms at the level of the descending thoracic aorta and supraceliac aorta showed pulsatile, antegrade flow throughout the cardiac cycle (**Figure 5**, right panel, blue lines). At the level of the infrarenal aorta, the flow waveform was less pulsatile, while still antegrade.

In the SAC model, high velocities and disturbed flow was observed at the brachiocephalic artery and aortic arch

Table 1. Lumped Parameter Model Values for the Calibrated Baseline Femoral Artery Cannulation Case

Vessel	Rp (g/mm^4·s)	C (mm^4·s^2/g)	Rd (g/mm^4·s)
1. Right subclavian artery	0.1163	0.3404	1.8227
2. Right common carotid artery	0.2761	0.3950	1.5646
3. Left common carotid artery	0.2761	0.3950	1.5646
4. Left subclavian artery	0.1163	0.3404	1.8225
5. Celiac trunk	0.0587	0.6598	0.9192
6. Superior mesenteric artery	0.0532	0.7312	0.8328
7. Right renal artery	0.1152	0.7993	0.6530
8. Right internal iliac artery	0.8088	0.0420	12.6704
9. Left internal iliac artery	0.8088	0.0420	12.6704
10. Right profunda femoral artery	0.8048	0.0420	12.6085
11. Left profunda femoral artery	0.8048	0.0420	12.6085
12. Right superficial femoral artery	0.2032	0.1681	3.1838
13. Left superficial femoral artery	0.2032	0.1681	3.1838

C, capacitance; Rd, distal resistance; Rp, proximal resistance.

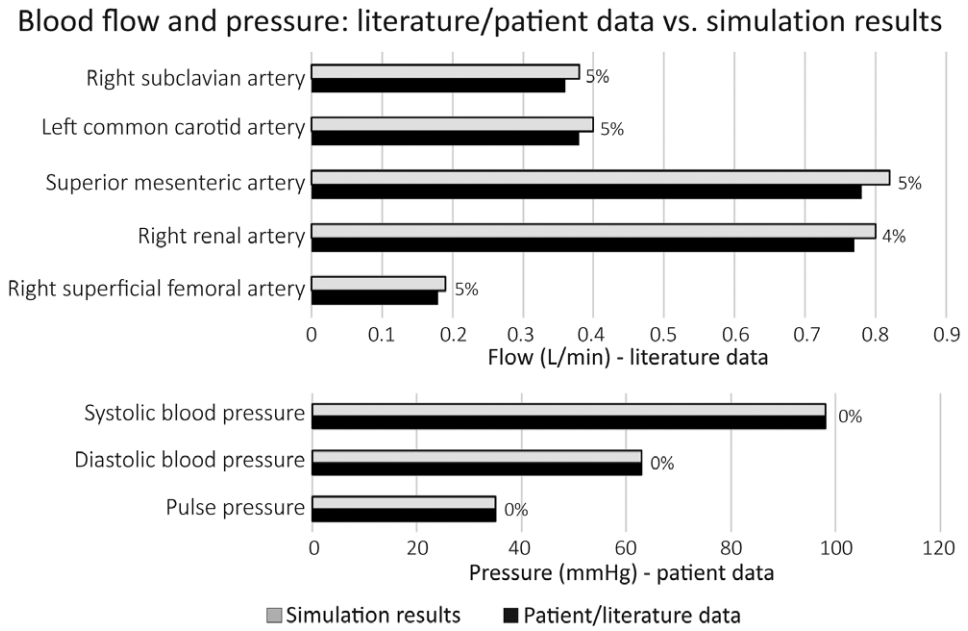

Figure 4. Comparison between literature data on flow splits, clinical data on blood pressure and the simulation results for the femoral artery cannulation model. Simulation results were matched within 5% of available clinical and literature data.

(**Figure 5**, left panel). Similar to the AAC model, peak-systolic and mid-diastolic velocity profiles through the thoracoabdominal aorta were antegrade. The flow waveforms at the level of the descending thoracic aorta and supraceliac aorta showed pulsatile, antegrade flow throughout the cardiac cycle (**Figure 5**, right panel, dashed red lines). At the level of the infrarenal aorta, the flow waveform was less pulsatile, while still antegrade.

TAWSS and OSI mapping for the different ECMO configurations are shown in **Figure 6**. In the FAC model the highest TAWSS was seen at the distal abdominal aorta, where the high-velocity jet of the arterial ECMO cannula hits the lateral wall of the aorta. The highest OSI was observed at the aortic arch and throughout descending thoracic aorta, in close proximity of the flow mixing zone at the aortic arch. In the AAC model, the highest TAWSS was seen at the posterolateral wall of the ascending aorta, while the highest OSI was observed at the anterolateral wall of the ascending aorta, around the arterial cannulation insertion. The SAC model simulations resulted in the highest TAWSS at the right subclavian and brachiocephalic artery, in line with the arterial ECMO cannula. The highest OSI was observed throughout the ascending aorta, aortic arch and brachiocephalic artery.

There were no significant differences in overall flow distribution to the aortic branch vessels or mean aortic pressures between the different ECMO cannulation configurations (Table, Supplemental Digital Contents 1 and 2, http://links.lww.com/ASAIO/A865).

Virtual Color-dye Analysis

In the FAC model, the mixing zone of cardiac and ECMO flows was located at the aortic arch (**Figure 7**). We found that most of the flow to the aortic arch vessels (70%) was cardiac driven. In contrast, the celiac trunk, superior mesenteric artery (SMA) and renal artery were completely supplied by ECMO-driven flow, as shown in Video 1 (Supplemental Digital Content 1, http://links.lww.com/ASAIO/A866). In the AAC model, as the arterial ECMO cannula was in close proximity to the heart, we observed a more homogenous mixing of flows, resulting

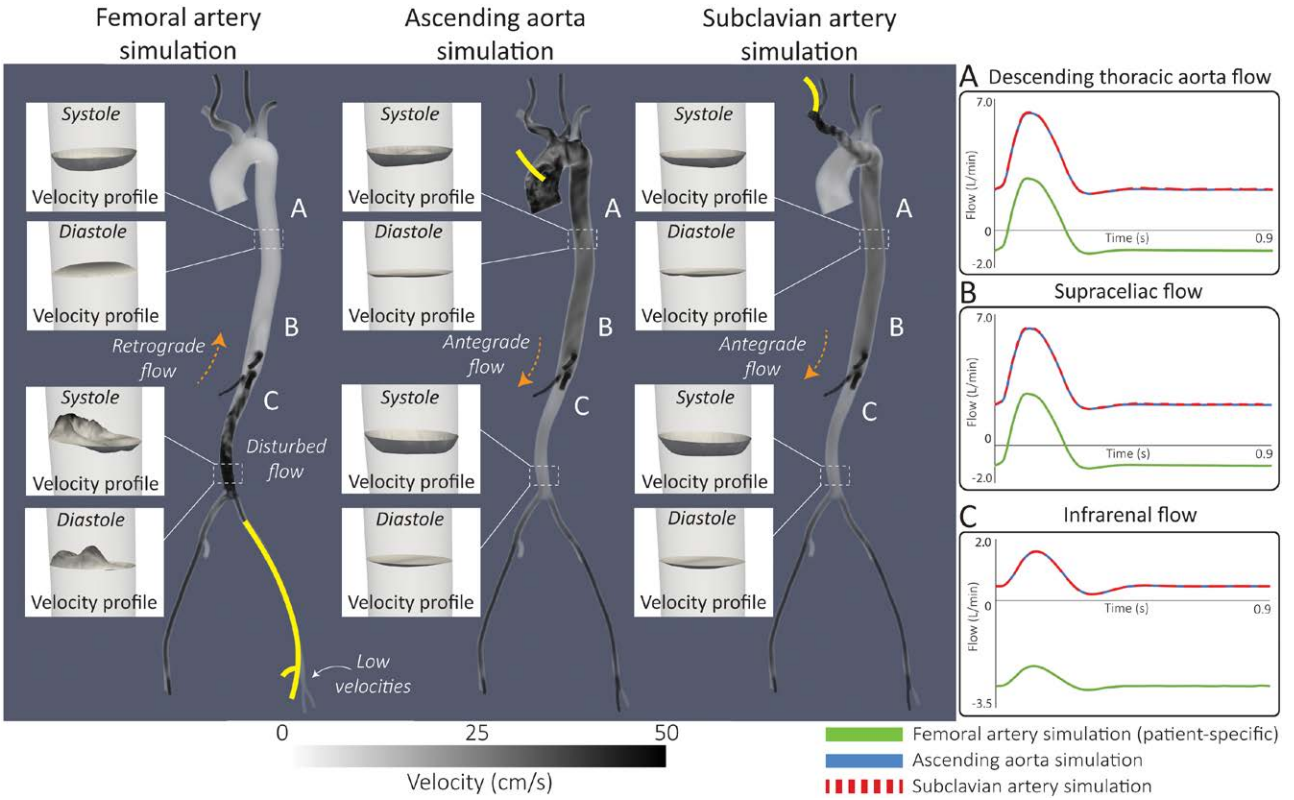

Figure 5. An assessment of global and regional flow characteristics for the 3 different ECMO configurations. Velocity renderings at peak systole and velocity profiles at peak systole and mid-diastole are shown in the left panel. The arterial ECMO cannula is in yellow. The right panel shows flow waveforms at various levels along the thoracoabdominal aorta. The femoral artery cannulation model is shown in the green lines, the ascending aorta cannulation model in the blue lines, and the subclavian artery cannulation model in the dashed red lines. ECMO, extracorporeal membrane oxygenation

in a balanced distribution of cardiac flow (~40%) and ECMO flow (~60%) throughout the vasculature. In the SAC model, flow from the LV was seen to be stagnant in the ascending aorta, where mixing was less efficient. The aortic arch vessels received most of the flow from the ECMO (84.5%), while the celiac trunk, SMA, and renal artery received approximately 71% of flow from the ECMO.

Discussion

ECMO hemodynamics are poorly understood as they represent an intricate interplay between pulsatile and steady-state flow.[10] In this work, we aimed to characterize complex blood flow in different ECMO configurations using an advanced, patient-specific CFD analysis. Further, we employed a novel virtual color-dye analysis to visualize and quantify contributions of cardiac and ECMO flows to the end-organ vascular beds. We found that pulsatile flow to the end-organ was maintained in a situation of predominantly nonpulsatile ECMO-driven hemodynamics. Differential contribution of cardiac and ECMO-derived flow to vascular beds was most notably observed in the FAC model, while the AAC and SAC models showed a more even distribution. Complex flow features in the different ECMO configurations resulted in various regions of high wall shear stress and oscillatory shear throughout the aorta.

In the FAC model, the mixing zone of native cardiac flow and steady-state ECMO flow was in the aortic arch. Consequently, the aortic arch vessels were predominantly supplied by cardiac flow. In case of pulmonary compromise, this poses a potential risk of differential upper body hypoxemia (Harlequin syndrome); a known complication of peripheral VA-ECMO.[3,5] The location of the watershed region is dependent on both cardiac output and level of ECMO support. Additionally, an animal study by Hou and colleagues found differential venous oxygen return to be a key contributor to upper body hypoxemia.[29] Previous computational studies, investigating the dynamic interaction between cardiac and ECMO flow, found that with increasing cardiac output, this mixing zone is shifted downstream into the descending thoracic aorta.[20] As a result, the aortic arch vessels were entirely perfused by the LV at ECMO support levels less than 75%. In both the SAC and AAC models we found that flows mixed in the proximal aorta, resulting in a balanced contribution of cardiac and ECMO-derived flows to the end-organ vascular beds, lowering the risk of differential hypoxemia. This finding is contrary to an earlier animal study by Kinsella and colleagues, in which they studied distribution of cardiac output and ECMO flow using microsphere bubbles.[30] In their study, the arterial ECMO cannula was placed in the ascending aorta. They did not find adequate flow mixing, but rather concluded that upper body flow was mainly ECMO driven, while the coronary arteries and the lower body were predominantly perfused by the left ventricle. Interestingly, in the AAC and SAC models, we note that although the ECMO flow rate is roughly three times larger compared with the native cardiac flow, this did not translate into a three times larger contribution to the various vascular beds compared with

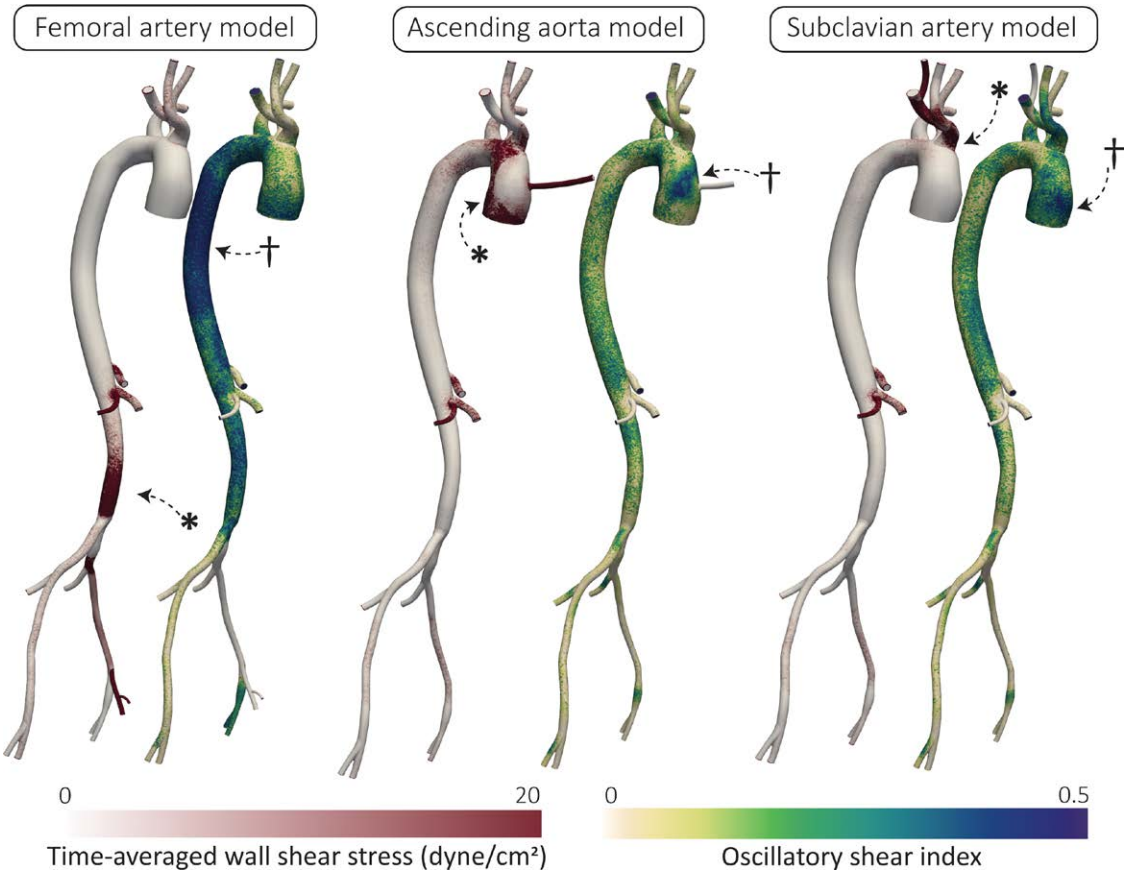

Figure 6. Analysis of TAWSS and OSI index for the 3 different ECMO configurations. Asterisk (*) depicts the region of highest TAWSS and cross (†) depicts the region of highest OSI. ECMO, extracorporeal membrane oxygenation; OSI, oscillatory shear; TAWSS, time-averaged wall shear stress.

native cardiac flow. A potential explanation for this observation could be inefficient arterial ECMO cannula angulation, leading to local flow stagnation.

The nonpulsatile ECMO flow constitutes the majority of the flow within the circulation; however, we found that the flow waveforms throughout the aorta and at all branch vessel maintained some level of pulsatility, albeit diminished in some vascular beds. While some pulsatile flow might be expected in the AAC and SAC models, given the proximal mixing of flows, we also observed pulsatile flow waveforms to the abdominal branch vessels that were completely supplied by ECMO flow in the FAC model. As studies have shown the association between nonpulsatile flow and end-organ microvascular dysfunction, it is important to note that native cardiac output, although low, has a distinct ability to impact pulsatility within the vasculature, even in end-organs that are completely supplied by ECMO flow.[31]

Although patients undergoing ECMO are systemically anticoagulated, thrombus formation in the ECMO circuit and arterial circulation remains an issue.[32] In the setting of complex geometries and blood flow patterns, the combination of wall shear stress and oscillatory shear can potentially lead to local endothelial dysfunction and thrombosis.[33] As reported by Seethararam and colleagues, complex flow features, including unsteady swirling, vortical flows, are encountered through the aorta due to the interaction between pulsatile cardiac flow and steady-state ECMO.[18] In our current study we found that the location of disturbed flow, and high wall shear stress co-localized with the insertion site of the arterial cannula, confirming previous findings by Nezami et al.[22] The peak oscillatory shear was located around the arterial cannula in the AAC and SAC model, most likely due to local recirculation of flow. The peak OSI for the FAC model was located in close proximity to the flow mixing zone the aortic arch. However, this region of the peak OSI was substantially larger compared with the AAC and SAC models, underlining the profound complex flow patterns observed in this specific ECMO configuration.

Study Limitations

Our work demonstrates the ability of computational modeling tools to provide in-depth assessment of complex flow features related to various ECMO configurations. While these findings may aid clinicians in providing adequate patient-specific ECMO management, several limitations exist. First, this is a single patient analysis, making it difficult to generalize the results put forward in this work. However, to effectively compare these different ECMO cannulation strategies, one would have to eliminate confounding variables of studies dealing with large patient cohorts, including varying anatomy, as well as flow and pressure conditions. Therefore, the strength of this advanced CFD analysis is the direct comparison of the hemodynamic impact of different ECMO cannulation strategies within the same patient. Second, the modeling assumptions in

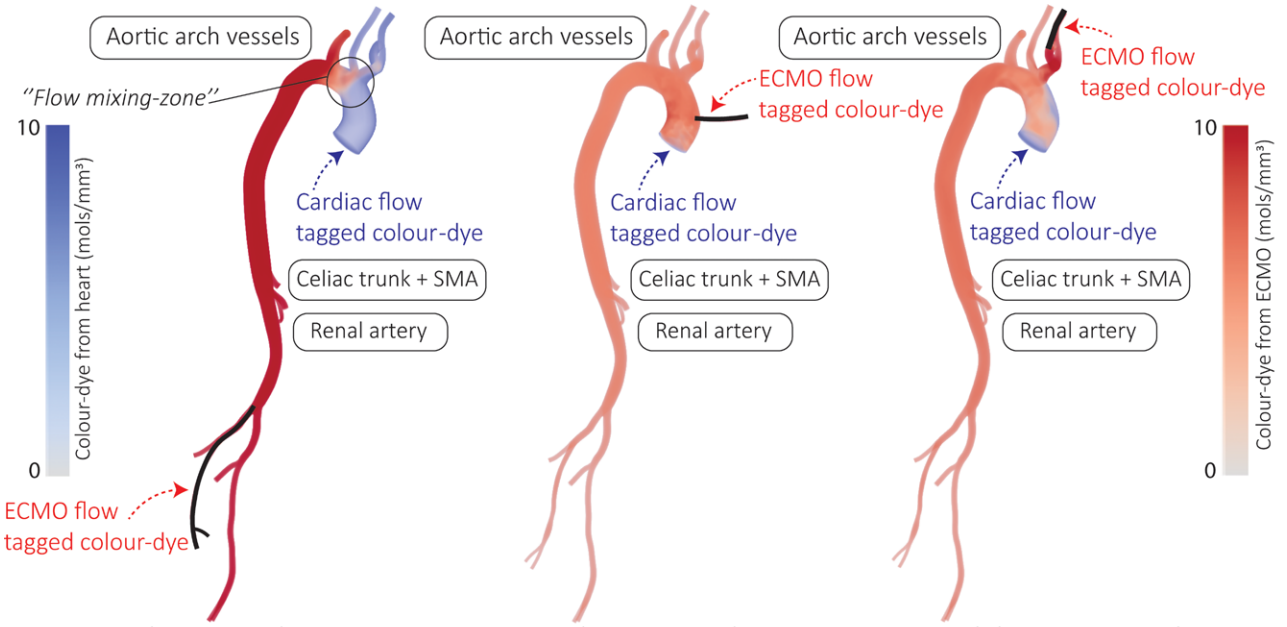

Femoral artery cannulation

Region	Cardiac flow	ECMO flow
Aortic arch vessels	70.0%	30.0%
Celiac trunk + SMA	0.0%	100%
Renal artery	0.0%	100%

Ascending aorta cannulation

Region	Cardiac flow	ECMO flow
Aortic arch vessels	38.7%	61.3%
Celiac trunk + SMA	38.2%	61.8%
Renal artery	38.2%	61.8%

Subclavian artery cannulation

Region	Cardiac flow	ECMO flow
Aortic arch vessels	15.5%	84.5%
Celiac trunk + SMA	28.9%	71.1%
Renal artery	28.6%	71.4%

Figure 7. We identified contributions of pulsatile and nonpulsatile flow to various end-organ vascular beds, including the aortic arch vessels, celiac trunk and SMA, and the renal artery, using virtual color-dye analysis. Flows were tagged with a dimensionless scalar, where cardiac-derived flow is labeled blue and ECMO-derived flow is labeled red. Simulation were run until cycle-to-cycle periodicity was achieved. ECMO, extracorporeal membrane oxygenation; SMA, superior mesenteric artery.

this study, including use of the same boundary conditions for the different ECMO configurations, do not take into account alterations to the systemic vascular resistance or cardiac output using pharmacological interventions, such as beta blockers, that might affect local blood flow and pressure. Third, while mesh independence was achieved for the pressure and flow waveforms in all configurations, ensuring mesh independent results for all the other quantities of interest (wall shear stress, oscillatory shear index, or the virtual color-dye analysis) would have increased the computational cost to an unfeasible limit, as was therefore not pursued. Fourth, while we were able to virtually assess the hemodynamic alteration introduced by the ascending aorta and subclavian artery ECMO configurations, we could not validate those hemodynamic outcomes with patient-specific clinical data.

Future Perspectives

We intend to build on this work and focus on assessment of ECMO-related hemodynamics in larger patient cohorts, including pediatric patients, with various ECMO configurations. Our computational analyses can be complemented by in-vitro studies consisting of mock circulation loops, as described by Rozencwajg and colleagues, from which we can incorporate additional data such as particle image velocimetry.[34] Further, we aim to explore pulmonary hemodynamics associated with VA-ECMO using 0D-3D closed loop computational models.[35] To obtain more insight on left ventricular function, we aim to set up a heart model that will give us the opportunity to study the impact of varying flow and pressure conditions on left ventricular stroke work and pressure-volume relationships, and thus provide meaningful information for clinical decision making regarding left ventricular unloading. To study thrombus related complications, we intend to employ previously described computational methods including scalar transport in combination with a Lagrangian Shearing metric termed platelet activation potential.[26] Finally, to explore optimal flow conditions in venoarterial ECMO, we aim to compare different arterial cannula designs with varying angulations and depths.

Conclusions

In conclusion, while global hemodynamics were relatively similar between ECMO configurations, several distinct hemodynamic indices, in particular wall shear stress and oscillatory shear patterns, as well as differential contribution of cardiac and ECMO flow to the various end-organ vascular beds, showed remarkable differences. The clinical impact of this study highlighting the relevance of CFD modeling in assessment of complex hemodynamics in ECMO warrants further evaluation.

References

1. Bartlett RH, Gazzaniga AB, Fong SW, Jefferies MR, Roohk HV, Haiduc N: Extracorporeal membrane oxygenator support for cardiopulmonary failure. Experience in 28 cases. *J Thorac Cardiovasc Surg* 73: 375–386, 1977.

2. Barbaro RP, MacLaren G, Boonstra PS, *et al*; Extracorporeal Life Support Organization: Extracorporeal membrane oxygenation support in COVID-19: An international cohort study of the Extracorporeal Life Support Organization registry. *Lancet* 396: 1071–1078, 2020.
3. Rao P, Khalpey Z, Smith R, Burkhoff D, Kociol RD: Venoarterial extracorporeal membrane oxygenation for cardiogenic shock and cardiac arrest. *Circ Heart Fail* 11: e004905, 2018.
4. Burrell AJC, Bennett V, Serra AL, *et al*; International ECMO Network (ECMONet): Venoarterial extracorporeal membrane oxygenation: A systematic review of selection criteria, outcome measures and definitions of complications. *J Crit Care* 53: 32–37, 2019.
5. Lorusso R, Shekar K, MacLaren G, *et al*: ELSO Interim guidelines for venoarterial extracorporeal membrane oxygenation in adult cardiac patients. *ASAIO J* 67: 827–844, 2021.
6. Lorusso R, Whitman G, Milojevic M, *et al*: 2020 EACTS/ELSO/STS/AATS expert consensus on post-cardiotomy extracorporeal life support in adult patients. *Ann Thorac Surg* 111: 327–369, 2021.
7. Rastan AJ, Dege A, Mohr M, *et al*: Early and late outcomes of 517 consecutive adult patients treated with extracorporeal membrane oxygenation for refractory postcardiotomy cardiogenic shock. *J Thorac Cardiovasc Surg* 139: 302–11, 311.e1, 2010.
8. Kowalewski M, Zieliński K, Brodie D, *et al*: Venoarterial extracorporeal membrane oxygenation for postcardiotomy shock—analysis of the extracorporeal life support organization registry. *Critical Care Medicine*. 2021; Publish Ah. doi:10.1097/ccm.0000000000004922
9. Djordjevic I, Eghbalzadeh K, Sabashnikov A, *et al*: Central vs peripheral venoarterial ECMO in postcardiotomy cardiogenic shock. *J Card Surg* 35: 1037–1042, 2020.
10. Burkhoff D, Sayer G, Doshi D, Uriel N: Hemodynamics of mechanical circulatory support. *J Am Coll Cardiol* 66: 2663–2674, 2015.
11. Zhang Y, Zeng J, He X, Cao W, Peng X, Li G. Pulsatility protects the endothelial glycocalyx during extracorporeal membrane oxygenation. *Microcirculation* 1–10, 2021.
12. Veraar CM, Rinösl H, Kühn K, *et al*: Non-pulsatile blood flow is associated with enhanced cerebrovascular carbon dioxide reactivity and an attenuated relationship between cerebral blood flow and regional brain oxygenation. *Crit Care* 23: 426, 2019.
13. Villa G, Katz N, Ronco C: Extracorporeal membrane oxygenation and the kidney. *Cardiorenal Med* 6: 50–60, 2015.
14. Lemétayer J, Broman LM, Prahl Wittberg L: Flow dynamics and mixing in extracorporeal support: A study of the return cannula. *Front Bioeng Biotechnol* 9: 630568, 2021.
15. Taylor CA, Figueroa CA: Patient-specific modeling of cardiovascular mechanics. *Annu Rev Biomed Eng* 11: 109–134, 2009.
16. Ahmed Y, Tossas-Betancourt C, van Bakel PAJ, *et al*: Interventional planning for endovascular revision of a lateral tunnel fontan: A patient-specific computational analysis. *Front Physiol* 12: 718254, 2021.
17. Tossas-Betancourt C, van Bakel TMJ, Arthurs CJ, *et al*: Computational analysis of renal artery flow characteristics by modeling aortoplasty and aortic bypass interventions for abdominal aortic coarctation. *J Vasc Surg* 71: 505–516.e4, 2020.
18. Seetharaman A, Keramati H, Ramanathan K, *et al*: Vortex dynamics of veno-arterial extracorporeal circulation: A computational fluid dynamics study. *Physics of Fluids* 33: 061908, 2021.
19. Feiger B, Adebiyi A, Randles A: Multiscale modeling of blood flow to assess neurological complications in patients supported by venoarterial extracorporeal membrane oxygenation. *Comput Biol Med* 129: 104155, 2021.
20. Stevens MC, Callaghan FM, Forrest P, Bannon PG, Grieve SM: Flow mixing during peripheral veno-arterial extra corporeal membrane oxygenation - A simulation study. *J Biomech* 55: 64–70, 2017.
21. Gu K, Zhang Y, Gao B, Chang Y, Zeng Y: Hemodynamic differences between central ECMO and peripheral ECMO: A primary CFD study. *Med Sci Monit* 22: 717–726, 2016.
22. Nezami FR, Ramezanpour M, Khodaee F, Goffer E, Edelman ER, Keller SP: Simulation of fluid-structure interaction in extracorporeal membrane oxygenation circulatory support systems. *J Cardiovasc Transl Res* 15: 249–257, 2022.
23. Arthurs CJ, Khlebnikov R, Melville A, *et al*: CRIMSON: An open-source software framework for cardiovascular integrated modelling and simulation. *PLoS Comput Biol* 17: e1008881, 2021.
24. Lantz BM, Foerster JM, Link DP, Holcroft JW: Regional distribution of cardiac output: Normal values in man determined by video dilution technique. *AJR Am J Roentgenol* 137: 903–907, 1981.
25. Xiao N, Alastruey J, Alberto Figueroa C: A systematic comparison between 1-D and 3-D hemodynamics in compliant arterial models. *Int J Numer Method Biomed Eng* 30: 204–231, 2014.
26. di Achille P, Tellides G, Figueroa CA, Humphrey JD. A haemodynamic predictor of intraluminal thrombus formation in abdominal aortic aneurysms. *Proc R Soc A Math Phys Eng Sci* 470: 20140163, 2014.
27. Ku DN, Giddens DP, Zarins CK, Glagov S: Pulsatile flow and atherosclerosis in the human carotid bifurcation. Positive correlation between plaque location and low oscillating shear stress. *Arteriosclerosis* 5: 293–302, 1985.
28. Lynch SR, Nama N, Xu Z, Arthurs CJ, Sahni O, Figueroa CA: Numerical considerations for advection-diffusion problems in cardiovascular hemodynamics. *Int J Numer Method Biomed Eng* 36: e3378, 2020.
29. Hou X, Yang X, Du Z, *et al*: Superior vena cava drainage improves upper body oxygenation during veno-arterial extracorporeal membrane oxygenation in sheep. *Crit Care* 19: 68, 2015.
30. Kinsella JP, Gerstmann DR, Rosenberg AA: The effect of extracorporeal membrane oxygenation on coronary perfusion and regional blood flow distribution. *Pediatr Res* 31: 80–84, 1992.
31. Salameh A, Kühne L, Grassl M, *et al*: Protective effects of pulsatile flow during cardiopulmonary bypass. *Ann Thorac Surg* 99: 192–199, 2015.
32. Hoyler MM, Flynn B, Iannacone EM, Jones MM, Ivascu NS: Clinical management of venoarterial extracorporeal membrane oxygenation. *J Cardiothorac Vasc Anesth* 34: 2776–2792, 2020.
33. Fuchs G, Berg N, Broman LM, Prahl Wittberg L: Flow-induced platelet activation in components of the extracorporeal membrane oxygenation circuit. *Sci Rep* 8: 13985, 2018.
34. Rozencwajg S, Wu EL, Heinsar S, *et al*. A mock circulation loop to evaluate differential hypoxemia during peripheral venoarterial extracorporeal membrane oxygenation [Published online January 17]. *Perfusion*. 2022. doi:10.1177/02676591211056567.
35. Silva Vieira M, Arthurs CJ, Hussain T, Razavi R, Figueroa CA: Patient-specific modeling of right coronary circulation vulnerability post-liver transplant in Alagille's syndrome. *PLoS One* 13: e0205829, 2018.